buildings

Article

Seismic Fragility Analysis of the Aging RC Columns under the Combined Action of Freeze–Thaw Cycles and Chloride-Induced Corrosion

Fengkun Cui [1], Linlin Song [1], Xingyu Wang [1], Mian Li [2], Peng Hu [1], Shuwen Deng [3], Xinyue Zhang [4] and Huihui Li [5,*]

1. Department of Civil Engineering, Shandong Jiaotong University, Jinan 250300, China
2. CCCC Second Harbor Engineering Company Ltd., Wuhan 430014, China
3. College of Water Resource & Civil Engineering, Hunan Agriculture University, Changsha 410083, China
4. School of Computer Science and Engineering, Tianjin University of Technology, Tianjin 300387, China
5. Guangdong Provincial Key Laboratory of Durability for Marine Civil Engineering, Shenzhen University, Shenzhen 518060, China

* Correspondence: lihuihui1015@szu.edu.cn

Abstract: The combined action of freeze–thaw cycles and chloride-induced corrosion are generally recognized as one of the main causes of the degradation of the mechanical properties and seismic performance of reinforced concrete (RC) structures in the northern frozen coastal regions. To investigate the degradation mechanisms of the seismic performance of RC columns subjected to the combined action of freeze–thaw cycles and chloride-induced corrosion, the impact of freeze–thaw cycles on the chloride diffusion coefficient of concrete was studied through concrete deterioration tests and theoretical analysis. This paper proposed a time-dependent deterioration model for RC columns, which is suitable to consider the combined action of freeze–thaw cycles and chloride-induced deterioration. The proposed deterioration model could be applied to the investigations of time-dependent seismic performance and the seismic fragility of RC columns. Based on the established deterioration model, this paper proposed a time-dependent seismic fragility analysis framework for the aging RC columns, considering the combined action of freeze–thaw cycles and chloride-induced corrosion. In addition, a representative three-span RC continuous T-shaped girder bridge that is located in the high-latitude northern frozen coastal regions of China was taken as the case study, and the time-dependent seismic fragility analysis of RC columns was conducted considering the involved uncertainties in geometric parameters, the deterioration mechanisms of the materials, and ground motions. The time-dependent seismic fragility curves of RC columns were obtained at different service time points. The results indicated that the combined action of freeze–thaw cycles and chloride-induced deterioration had a significant influence on the time-dependent seismic responses of the deteriorating RC columns. Under the combined action of freeze–thaw cycles and chloride-induced corrosion, when the RC bridge was in service for 75 years, the stirrup strength decreased by 3.88% and the cross-sectional area decreased by 30.03%. The peak stress of the confined concrete decreased by 52.1% and its peak strain increased by 12.2 times, respectively. Moreover, the time-dependent seismic fragilities of the aging RC columns under different damage states exhibited a nonlinear increase as the service life increased.

Keywords: seismic performance; RC columns; the combined action of freeze–thaw cycles and chloride-induced corrosion; deterioration model; material degradation mechanisms; time-dependent seismic fragility curves

Citation: Cui, F.; Song, L.; Wang, X.; Li, M.; Hu, P.; Deng, S.; Zhang, X.; Li, H. Seismic Fragility Analysis of the Aging RC Columns under the Combined Action of Freeze–Thaw Cycles and Chloride-Induced Corrosion. *Buildings* **2022**, *12*, 2223. https://doi.org/10.3390/buildings12122223

Academic Editor: Flavio Stochino

Received: 15 November 2022
Accepted: 12 December 2022
Published: 14 December 2022

1. Introduction

For the reinforced concrete (RC) highway bridges that are located in the northern high-latitude frozen coastal regions, their service conditions, such as the freezing weather conditions and harsh marine environment, are very complicated. As the critical structural components of these RC highway bridges that are working in the northern frozen coastal areas, RC columns are extremely prone to long-term freeze–thaw cycles and chloride-induced deterioration during their service life. Due to the combined action of long-term freeze–thaw cycles and chloride-induced corrosion, RC columns could be severely damaged, as shown in Figure 1, and the mechanical properties of the concrete and reinforcing steel, as well as the structural resistance and load-carrying capacity of the RC columns could be degraded. This would further impair the durability and long-term service ability of RC highway bridges that are located in northern high-latitude frozen coastal regions [1–3]. Meanwhile, if such highway bridges are also located in seismic-prone areas, the combined effects of freeze–thaw cycles and chloride-induced corrosion may not only deteriorate the seismic capacity of RC columns, but also lead to the relevant modifications in their structural stiffness and damping. These deteriorations and modifications would further result in changes in the dynamic characteristics and the seismic performance of RC columns under earthquake excitations. Therefore, it is necessary to investigate the time-variant seismic performance of RC columns for the highway bridges that are located in the northern high-latitude frozen coastal regions, considering the combined action of freeze–thaw cycles and chloride-induced deterioration [4,5].

Figure 1. Damage modes of RC columns due to the combined action of freeze–thaw cycles and chloride-induced corrosion.

To make a relatively accurate evaluation of the time-dependent seismic performance and seismic fragility of RC columns in the northern frozen coastal regions over their service period, it is necessary to consider the combined effects of freeze–thaw cycles and chloride-induced deterioration. To date, many scholars have studied the effects of freeze–thaw cycles and chloride-induced corrosion on the time-dependent seismic performance of RC structures. Firstly, for studies focused on freeze–thaw damage on the mechanical properties of concrete, Cao et al. [6] investigated the mechanical properties of the freeze–thawing damage to concrete based on the freshwater freeze–thaw conditions, and they found that the mechanical features of freeze–thawing-damaged concrete decreased gradually with the increase in freeze–thaw cycles. Liu et al. [7] analyzed the seismic performance of concrete columns after freeze–thaw cycles according to the damage modes, load-displacement relationships, ductility, and stiffness degradation of the concrete columns. Xu et al. [8] investigated the seismic performance of RC columns after freeze–thaw cycles, and they found that the cumulative energy dissipation capacity of RC columns continued to decrease due to the coupling effects of material degradation and bond loosening. Hanjari [9] also suggested that the mechanical properties and seismic performance of RC members would deteriorate over time due to the gradual deterioration of the durability of concrete and steel reinforcements. Subsequently, based on the aforementioned studies, Zheng et al. [10] proposed a law describing the degradation of the seismic performance of RC columns under different freeze–thaw cycles through quasi-static loading tests. Hasan et al. [11] investigated the changes in the mechanical properties of concrete after freeze–thaw cycles, and they also proposed a concrete constitutive relationship for freeze–thaw-damaged concrete based on the plastic strain behavior of concrete. Berto et al. [12] suggested a freeze–thaw mechanical damage model that considered the effects of freeze–thaw cycles on the degradation of the structural behavior of RC structures.

Moreover, many studies also investigated the effect of chloride-induced corrosion on the mechanical properties of RC structures. For instance, Shen et al. [13] investigated the combined effects of chloride-induced corrosion and carbonization on RC structures in the marine environment, and they found that both chloride-induced corrosion and carbonization could lead to the deterioration of steel reinforcements and concrete. Guo et al. [14] studied the effect of chloride-induced corrosion on the seismic behavior of RC columns. They demonstrated that the degradation of the seismic performance of RC columns increased significantly with the corrosion degree of chloride-induced deterioration. Ou et al. [15] proposed a seismic evaluation method for corroded RC bridges based on the nonlinear static pushover analysis, considering the corrosion of steel caused by chloride-induced deterioration. On the other hand, according to several previous studies [16–21], it has been found that the probability of steel reinforcement deterioration caused by the chloride-induced corrosion of RC columns was also as higher than that of concrete deterioration. Thus, the effect of chloride-induced corrosion on the degradation of the mechanical properties and seismic fragility estimates of RC columns should be carefully considered.

In summary, based on the above-mentioned comprehensive literature review, most of the previous studies mainly focused on the effects of single freeze–thaw cycles or chloride-induced corrosion only on the deterioration of the mechanical properties and seismic performance of the aging RC columns or other RC structures, whereas relatively very rare studies focused on investigating the combined action of freeze–thaw cycles and chloride-induced corrosion on the mechanical characteristics, seismic responses, and seismic fragility assessments of the aging RC structures. Furthermore, there are still very few available analytical models applied in the field of seismic analysis for deteriorating RC columns, considering the combined action of freeze–thaw cycles and chloride-induced corrosion. Therefore, the question of how to establish and propose a general time-dependent deterioration model taking into consideration the combined action of freeze–thaw cycles and chloride-induced corrosion is an important matter to investigate, and it could provide certain potential value in engineering applications and be of great importance for the assessment of seismic responses and time-dependent seismic fragility estimates for the aging RC columns of highway bridges that are located in the northern frozen coastal regions.

In the present study, mechanical and permeability resistance tests, as well as the microscopic structure analysis of a series of concrete specimens were first performed to study the combined action of freeze–thaw cycles and chloride-induced corrosion on RC structures. The conversion relationship between the number of freeze–thaw cycles in laboratory conditions and the average annual freeze–thaw cycles of practical regions that the concrete specimens were located in was also considered. Then, based on the existing deterioration model, the time-dependent deterioration model of RC structures under the combined action of freeze–thaw cycles and chloride-induced corrosion was developed. Subsequently, to verify the effectiveness and feasibility of the proposed deterioration model of RC structures, this paper proposed a time-dependent seismic fragility assessment framework, considering the uncertainties involved in the degradation of material properties, structural geometries, and ground motions. In addition, by taking a typical three-span RC continuous T-shaped girder bridge that is located in the high-latitude northern frozen coastal regions of China as a case study, the time-dependent seismic fragility estimates of RC columns under the combined action of freeze–thaw cycles and chloride-induced deterioration were carried out. Finally, the time-dependent seismic fragility curves of RC columns were developed at different service times. The results obtained from this paper may provide certain possible references for those studying the degradation of the mechanical properties and seismic performance of, and carrying out time-dependent seismic vulnerability assessments on the aging RC columns that are located in the northern coastal regions or in service in complicated freeze–thaw marine environments, where the combined action of long-term freeze–thaw cycles and chloride-induced corrosion are often involved.

2. Deterioration Model of RC Structures under the Combined Action of Freeze–Thaw Cycles and Chloride-Induced Corrosion

2.1. Concrete Deterioration Test Results and Analysis

2.1.1. Test Scheme

To investigate the mechanical properties of concrete under the combined action of freeze–thaw cycles and chloride-induced corrosion, mechanical tests on a series of concrete specimens were carried out. In addition, to study the influence of freeze–thaw cycles on the chloride ion diffusion coefficient in concrete, the chloride ion permeability test was also performed. According to the Standard for Test Methods for Long-Term Performance and Durability of Ordinary Concrete [22], several standard coupon test specimens of the C40 concrete with the dimensions of 100 mm × 100 mm × 400 mm were prepared. After the standard curing of these specimens for 28 days until they reached a standard compressive strength, the rapid freeze–thaw testing of the concrete specimens was conducted in a 3.5% NaCl solution. After 0, 50, 100, 150, and 200 freeze–thaw cycles, respectively, the mechanical property tests and chloride ion permeability tests of the specimens were conducted, respectively.

2.1.2. Materials and Work Method

In this paper, the C40 concrete is used in the concrete deterioration test. Its composition includes Portland cement, mineral powder, fly ash, fine aggregate, coarse aggregate, water, and water-reducing agent. Fine aggregate is river sand, coarse aggregate is granite gravel, and the coarse aggregate particle size ranges are 5–10 mm and 10–20 mm, respectively. The mixture proportion of the C40 concrete is shown in Table 1.

Table 1. Mixture proportion of the C40 concrete.

Portland Cement	Mineral Powder	Fly Ash	Fine Aggregate	Coarse Aggregate		Water	Water Reducing Agent
				5–10 mm	10–20 mm		
8.5%	3.65%	8.1%	30.45%	13%	30.3%	5.5%	0.5%

A forced concrete mixer (HJW-60, produced by Cangzhou Ouhai Testing Instruments Co., Cangzhou, China) was used for concrete mixing, and the concrete was loaded into the cast iron mold after the mixing was completed. A concrete rapid freeze–thaw testing machine (HC-HDK, produced by Jianyan Huace Instrument and Equipment Co., Beijing, China) was used for the freeze–thaw tests. The freeze–thaw temperature range was 5~−18 °C, the time of a single freeze–thaw cycle was 3.2 h, and the cooling rate was 15 °C/h. The peak stress, peak strain, and modulus of elasticity of the concrete were obtained from the stress–strain curves measured by the electro-hydraulic servo pressure-testing machine (CTS-P5000, produced by Jinan Quanli Testing Technology Co., Jinan, China). Chloride ion permeation tests were performed by using the chloride ions migration coefficient gauge (RCM-6T, produced by Beijing Shuzhi Yilong Instrument Co., Beijing, China), according to the rapid chloride migration (RCM) method, to measure the chloride ion diffusion coefficient of concrete.

The concrete specimens were tested for 0, 50, 100, 150, and 200 freeze–thaw cycles, of which 4 specimens were tested for each group of freeze–thaw cycles. After the freeze–thaw cycle test, the specimens were made into 100 mm × 100 mm × 100 mm cubic and 100 mm × 50 mm cylindrical specimens. The three cubic specimens were taken for the mechanical property tests, and the three cylindrical specimens were taken for the chloride ion penetration tests, respectively. The test process is shown in Figure 2.

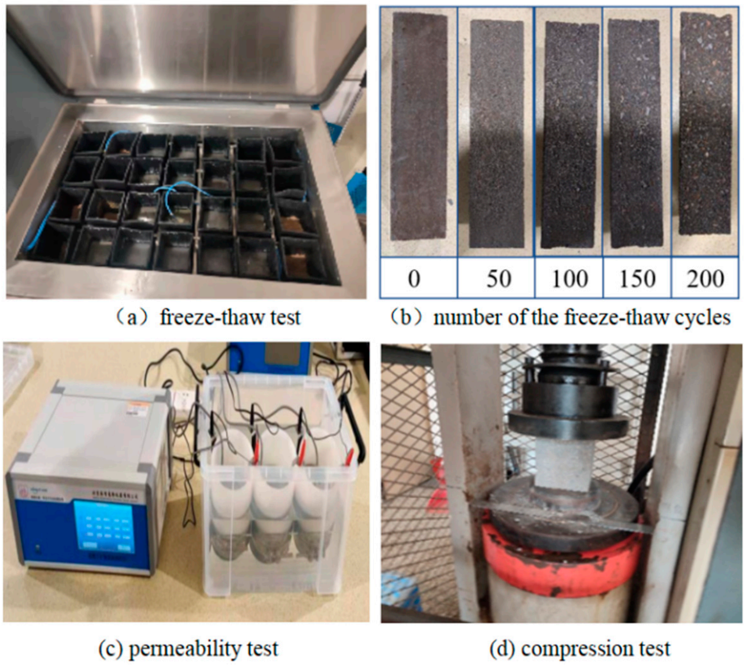

Figure 2. Procedures of the concrete deterioration tests. (**a**) freeze–thaw test; (**b**) number of the freeze–thaw cycles; (**c**) permeability test; (**d**) compression test.

2.1.3. Test Results of the Macro-Structures

The peak stress, peak strain, and elastic modulus of the concrete specimens under the combined action of freeze–thaw cycles and chloride-induced corrosion were measured. Meanwhile, the diffusion coefficients of chloride ions were also obtained for different freeze–thaw cycles, which lays a foundation for the construction of the deterioration model of RC structures subjected to the combined action of freeze–thaw cycles and chloride-induced deterioration. The corresponding test results are shown in Table 2.

Table 2. Experimental test results of the concrete deterioration tests.

Number of Freeze–Thaw Cycles	Peak Stress f_{co} (MPa)	Standard Deviation for f_{co}	Peak Strain ε_{co}	Standard Deviation for ε_{co}	Modulus of Elasticity E_c (10^4 MPa)	Standard Deviation for E_c	Chloride Ion Diffusion Coefficients D (10^{-12} m^2/s)	Standard Deviation for D
0	45	1.755	0.002	0.000094	3.25	0.1495	1.003	0.0481
50	36.4	1.529	0.0058	0.000282	2.65	0.1272	1.664	0.0865
100	28.7	1.263	0.0065	0.000345	2.41	0.1253	2.247	0.1258
150	25.6	1.229	0.010	0.00055	2.20	0.1188	2.669	0.1655
200	20.3	1.035	0.017	0.00102	1.95	0.1151	4.433	0.2926

Note: The coefficients of variation in the table are from three sets of test samples.

As seen from Table 2, with the increase in freeze–thaw cycles, the mechanical properties of the concrete and its resistance to chloride-induced corrosion continued to decrease. After many freeze–thaw cycles, small cracks inside the concrete began to expand, increasing the porosity inside the concrete. Therefore, the peak stress and elastic modulus of concrete decreased with the increase in freeze–thaw cycles, whereas the peak strain increased as the number of freeze–thaw cycles increased. After 100 freeze–thaw cycles, the peak stress of concrete decreased by 36%, the elastic modulus decreased by 26%, and the peak strain increased by 8.5 times, respectively. Moreover, due to the gradual removal of the concrete skin and external aggregate, an accelerated rate of chloride-induced corrosion on the concrete was also observed during the tests. After 100 Freeze–thaw cycles, the diffusion coefficient of chloride ions increased by 2.24 times, while it increased by 4.42 times after 200 freeze–thaw cycles.

2.1.4. Test Results of the Micro-Structures

To explore the influence mechanism of the combined action of freeze–thaw cycles and chloride-induced corrosion on the internal crack change and mechanical properties of the concrete, the cement slurry peeled from the concrete specimens after freeze–thaw cycles was ground into powder and then scanned by using the Scanning Electron Microscope (SEM), as shown in Figure 3.

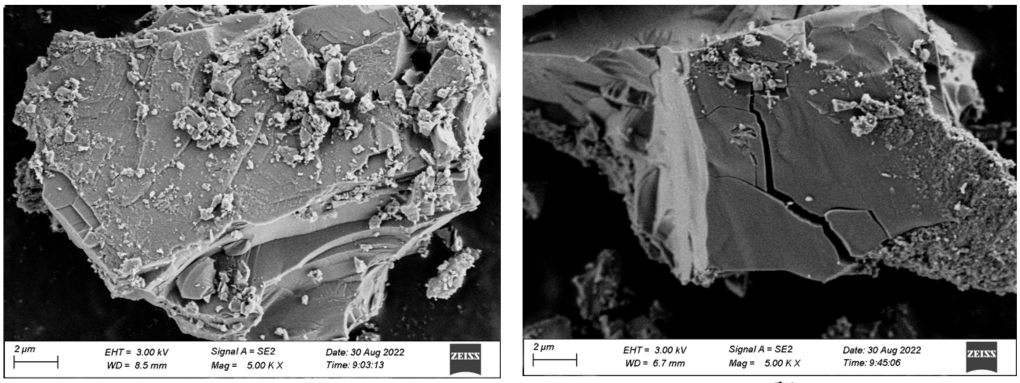

(a) (b)

Figure 3. Internal micro-structure of the concrete specimens after 0 (**a**) and 150 (**b**) freeze–thaw cycles.

The internal micro-structure of the concrete specimens was observed by a 5000x SEM, as shown in Figure 3. With the increase in the number of freeze–thaw cycles, the number width of cracks increased rapidly. As seen in Figure 3a, there were many micro-cracks and pores inside the micro-structure of the unfreeze–thawing concrete after solidification. These microscopic cracks and pores were parts of the initial damage, and they did not affect the deterioration performance of the concrete. However, when the number of freeze–thaw cycles reached 150, the crack width became larger, the micro-cracks gathered, and the hydration products were relatively loose, as seen in Figure 3b. Thus, it is demonstrated that the mechanical properties of the concrete under the combined action of freeze–thaw cycles and chloride-induced corrosion continued to decrease with the increase in the number of freeze–thaw cycles. Meanwhile, the resistance to chloride ion attacks was also gradually degraded.

2.2. Corrosion Initiation Time of Steel

Many previous studies [23–29] have shown that the diffusion process of chloride ions in concrete structures can usually be expressed by using Fick's second law, which can be expressed as

$$\frac{C(x,t)}{\partial t} = -\frac{\partial}{\partial x}\left[D\frac{\partial C(x,t)}{\partial t}\right] \tag{1}$$

where $C(x,t)$ is the chloride concentration of the concrete at the depth of x at time t; D is the chloride ion diffusion coefficient; x is the depth from the concrete surface; and t is the chloride ion diffusion time. Given the boundary conditions of $C(x,t) = C_0$, $C(\infty,t) = C_0$, and the initial condition of $C(x,t) = C_0$, the chloride concentration can be determined by

$$C(x,t) = C_0 + (C_s - C_0)(1 - erf\frac{x}{2\sqrt{Dt}}) \tag{2}$$

where C_0 is the initial chloride concentration; C_s is the chloride concentration on the concrete surface; and $erf(\cdot)$ is the Gaussian error function, which can be expressed as

$$erf(z) = \frac{2}{\sqrt{\pi}} \int_0^z e^{-u^2} du \quad (3)$$

The diffusion coefficient of chloride ions is closely related to time. With the increase in time, the cementitious material in concrete is continuously hydrated and the total porosity decreases, leading to a gradual decrease in the chloride ion diffusion coefficient. According to the Life-365 model suggested in [30], the influence of age on the chloride ion diffusion coefficient can be expressed as $D_{ref}(\frac{t_{ref}}{t})^m$, and the diffusion coefficients related to time t and temperature T can be expressed as

$$D(t) = D_{ref}(\frac{t_{ref}}{t})^m \cdot \exp\left[\frac{U}{R}(\frac{1}{T_{ref}} - \frac{1}{T})\right] \quad (4)$$

where D_{ref} is the chloride ion diffusion coefficient at time t_{ref} (the default value is 28 days) and temperature t_{ref} (the default value is 293 K); m is the diffusion coefficient attenuation index; U is the activation energy (35000 J/mol); R is the gas constant (8.314 J/mol·K); and T is the temperature. By substituting Equation (4) into Equation (2), we can further obtain the chloride concentration as

$$C(x,t) = C_0 + (C_s - C_0)\left(1 - erf\frac{x}{2\sqrt{D_{ref}t_{ref}{}^m t^{1-m} \cdot \exp\left[\frac{U}{R}(\frac{1}{T_{ref}} - \frac{1}{T})\right]}}\right) \quad (5)$$

The Life-365 model suggested in [30] does not consider the effect of freeze–thaw cycles on the diffusion rate of chloride ions in concrete structures. The acquired test results in Section 2.1 indicated that the rate of chloride ion diffusion increased with the increase in freeze–thaw cycles. Therefore, a freeze–thaw influence parameter was introduced into the Life-365 model [30] to establish the chloride ion diffusion coefficient model under cyclic freeze–thaw damage. According to the experimental data of the chloride ion diffusion coefficient in the concrete specimens after freeze–thaw cycles, variations in the chloride ion diffusion coefficient of the concrete versus the number of freezing-thawing cycles were obtained through data fitting, as shown in Figure 4.

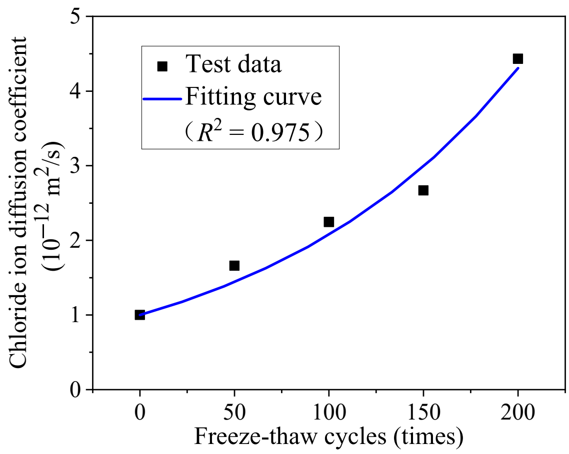

Figure 4. Fitting results for the chloride ion diffusion coefficient of the concrete under freeze–thaw cycles.

At present, a large number of scholars have carried out relevant freeze–thaw tests to explore the variation laws of the chloride ion diffusion coefficient under different freeze–thaw cycles [31–33]. There are many uncertain factors involved in the test process, such as different test conditions, different equipment performance, and personnel operation errors. Therefore, it is not reasonable to establish a fitting model using the test data collected from the other literature directly. However, it can be seen from Figure 4 that the law of the fitting results fits well with the laws suggested in other studies [31–33]. The peak stress of the concrete increases with the increase in freeze–thaw cycles in an exponential way, which further verifies the rationality and reliability of the fitting results. According to the data fitting results, the variation law of the concrete chloride ion diffusion coefficient, as a function of f_D $(\cdot)$, with the freeze–thaw cycles, N, was obtained as

$$f_D = e^{0.0073011N} \tag{6}$$

According to [34], the conversion relationship between the number of laboratory freeze–thaw cycles (N) and the actual annual average ([N]) could be expressed as N = 12[N]. To establish the function of f_D (t) reflecting the effect of freeze–thaw cycles on concrete structures under practical conditions, the function f_D (t) can be determined by

$$f_D(t) = e^{0.0073011\frac{[N]t}{12}} \tag{7}$$

Then the impact of freeze–thaw damage on the chloride ion diffusion coefficient of the concrete structures can be expressed as

$$D = D_{ref} \cdot f_D(t) \tag{8}$$

Finally, a new model of the chloride diffusion coefficient of the concrete structures under freeze–thaw cycles was established, which can be expressed as

$$C(x,t) = C_0 + (C_s - C_0) \cdot \left(1 - erf \frac{x}{2\sqrt{D_{ref} {t_{ref}}^m t^{1-m} \cdot \exp\left[\frac{U}{R}\left(\frac{1}{T_{ref}} - \frac{1}{T}\right)\right] \cdot e^{0.0073011\frac{[N]t}{12}}}} \right) \tag{9}$$

Moreover, according to [35], steel surface corrosion occurs when the chloride concentration on the surface of steel reaches a critical value of C_{cr}, and this specific time point is known as the corrosion initiation time of steel (t_{corr}). Since t_{corr} is implied in the chloride ion diffusion coefficient model, it should be solved by using numerical methods.

2.3. Time-Dependent Corrosion Mechanisms of Steel Rebar

2.3.1. Corrosion Rate of Steel Rebar

For a given RC structure subjected to the combined action of freeze–thaw cycles and chloride-induced corrosion, the time-dependent corrosion rate of steel (λ) can be expressed as [36,37]

$$\lambda(t) = 0.0115 \cdot i_{corr}(t) \tag{10}$$

where $i_{corr}(t)$ is the time-dependent corrosion current density, which can be written as [38]

$$i_{corr}(t) = 0.85 i_{corr,0}(t - t_{corr}), t > t_{corr} \tag{11}$$

where $i_{corr,0}$ is the corrosion current density at the initial corrosion (t = 0) [38], and its value is related to the water–cement ratio (w/b) of concrete and the protective layer thickness d_c. It can be calculated by the following formula.

$$i_{corr,0} = \frac{37.8(1 - w/b)^{-1.64}}{d_c} \tag{12}$$

2.3.2. Residual Cross-Sectional Area of Steel

The uniform corrosion depth of steel can be determined by the integration of the corrosion rate of steel, so the residual diameter of steel bars, $d_s(t)$, at time point t can be computed as [38]

$$d_s(t) = d_{s0} - 2\int_{t_{corr}}^{t} \lambda(t)dt \tag{13}$$

where d_{s0} is the initial diameter of steel rebar prior to the corrosion initiation time of steel in mm, and $\lambda(t)$ is the corrosion rate of steel at time point t in $\mu A/cm^2$. Thus, the residual cross-sectional area of steel bars under the case of uniform corrosion can be further expressed as

$$A_r(t) = \frac{\pi \cdot [d_s(t)]^2}{4} \tag{14}$$

2.3.3. Steel Strength

Steel strength is an important indicator of the mechanical properties of steel rebar. Chloride-induced corrosion can cause the degradation of steel strength. According to the experimental results in Du et al. [39], the reduction in the yield strength of steel rebar along the service life of RC structures can be expressed as

$$f_y(t) = (1 - 0.005 \cdot Q_{corr}(t))f_{y0} \tag{15}$$

where f_{y0} is the initial yield strength of steel rebar; $Q_{corr}(t)$ is the time-dependent corrosion percentage of steel rebar in terms of the cross-sectional area loss, which can be written as

$$Q_{corr} = \frac{A_{s0} - A_r(t)}{A_{s0}} \times 100 \tag{16}$$

2.3.4. Steel Ductility

Chloride-induced corrosion could also deteriorate the ductility of steel rebar, which can be expressed as the ratio of the ultimate strain (ε_u) to the yield strain (ε_y) of steel rebar, which can in turn be expressed as [40,41]

$$\frac{\varepsilon_u}{\varepsilon_y}(t) = [1 - 0.0136 \cdot Q_{corr}(t)] \cdot \frac{\varepsilon_{u0}}{\varepsilon_{y0}} \tag{17}$$

where ε_{u0} and ε_{y0} are the initial ultimate and yield strains of steel rebar, respectively.

2.4. The Proposed Time-Dependent Deterioration Model of RC Structures under the Combined Action of Freeze–Thaw Cycles and Chloride-Induced Corrosion

2.4.1. Traditional Mander Constitutive Model

The Mander constitutive model is often used in the numerical simulations of concrete structures (i.e., the confined concrete) [42,43], which can be represented by

$$f_c = \frac{f'_{cc} \cdot x \cdot r}{r - 1 + x^r} \tag{18}$$

$$x = \frac{\varepsilon_c}{\varepsilon_{cc}} \tag{19}$$

$$\varepsilon_{cc} = \varepsilon_{cc} \cdot \left[1 + 5 \cdot \left(\frac{f'_{cc}}{f'_{co}} - 1\right)\right] \tag{20}$$

$$r = \frac{E_c}{E_c - E_{sec}} = \frac{E_c}{E_c - \left(\frac{f'_{cc}}{\varepsilon}\right)} \tag{21}$$

$$f'_{cc} = f'_{co} \cdot \left(-1.254 + 2.254\sqrt{1 + \frac{7.94 f'_l}{f'_{co}}} - \frac{2 f'_l}{f'_{co}} \right) \tag{22}$$

where f_c is the compressive strength of concrete; f'_{cc} is the peak stress of the confined concrete; f'_{co} is the peak stress of the cover concrete; f'_l is the effective lateral confining stress provided by the stirrups to concrete; ε_c is the compressive strain of concrete; ε_{cc} is the compressive strain of concrete corresponding to the peak stress of the confined concrete; E_c is the elastic modulus of concrete; and E_{sec} is the secant modulus of concrete, respectively, according to [44]. Then, based on Equations (18)–(22), the traditional Mander constitutive model can be expressed as

$$f_c = \frac{f'_{cc} \cdot \left(\frac{\varepsilon_c}{\varepsilon_{cc}}\right) \cdot r}{r - 1 + \left(\frac{\varepsilon_c}{\varepsilon_{cc}}\right)^r} \tag{23}$$

According to Sun et al. [45], the combined action of freeze–thaw cycles and chloride-induced corrosion may lead to the deterioration of the structural performance of RC structures. In addition, the traditional Mander constitutive model is only applicable to the stress–strain relationship of concrete under monotonic loading at slow strain rates [42]. However, for these RC structures under the combined action of freeze–thaw cycles and chloride-induced deterioration, the traditional Mander constitutive model could not be directly used to simulate these RC members under such combined action. Thus, to accurately simulate the mechanical and structural responses of RC structures under the combined action of freeze–thaw cycles and chloride-induced corrosion, it is necessary to modify the conventional Mander constitutive model and establish an improved constitutive model considering the combined action of freeze–thaw cycles and chloride-induced deterioration.

2.4.2. The Modified Mander Constitutive Model

In this paper, the combined action of freeze–thaw cycles and chloride-induced corrosion on RC structures was introduced into the widely utilized traditional Mander constitutive model according to the change in the parameter as a function of time. Thus, the relationship between the proposed modified Mander constitutive model and the traditional one of RC structures could be expressed as

$$f_{c,m} = \frac{f'_{cc,m} \cdot \frac{\varepsilon_{c,m}}{\varepsilon_{cc,m}} \cdot r_m}{r_{cp} - 1 + \left(\frac{\varepsilon_{c,m}}{\varepsilon_{cc,m}}\right)^{r_m}} \tag{24}$$

where $f_{c,m}$ is the modified compressive strength of concrete; $f'_{cc,m}$ is the modified peak stress of the confined concrete; $\varepsilon_{c,m}$ is the modified compressive strain of the unconfined concrete; $\varepsilon_{cc,m}$ is the modified compressive strain of concrete corresponding to the modified peak stress of the confined concrete; and r_m is the modified member shape parameter, respectively. The derivations of these modified parameters were introduced in the following subsections.

(1) The modified peak stress of the confined concrete ($f'_{cc,m}$)

Based on the obtained experimental results, the variations of the peak stress of the concrete under different freeze–thaw cycles were fitted, as shown in Figure 5.

To date, many previous studies have carried out different freeze–thaw damage tests to explore the change law of the peak stress of concrete under different freeze–thaw cycles [3,11,46]. There are many uncertain factors in the test process, such as the difference in concrete raw materials, the size and shape of the specimens, different material ratios, different performance of the equipment, and the operation error of the personnel. Therefore, it is not reasonable to establish a fitting model using the test data collected from the other literature directly. However, it can be seen from Figure 5 that, the law of fitting results has a good match with the laws shown in other studies [3,11,46]. The peak stress of concrete decreases with the increase in freeze–thaw cycles in an exponential form, which further verifies the rationality and reliability of the fitting results. Based on the fitting results of the experimental results in Figure 5, a function reflecting the influence of freeze–thaw cycles on the concrete peak stress under realistic conditions as a function of time t (years) is expressed as

$$f'_{co,m} = 44.6 \cdot e^{\frac{-0.003966 \cdot [N] \cdot t}{12}} \tag{25}$$

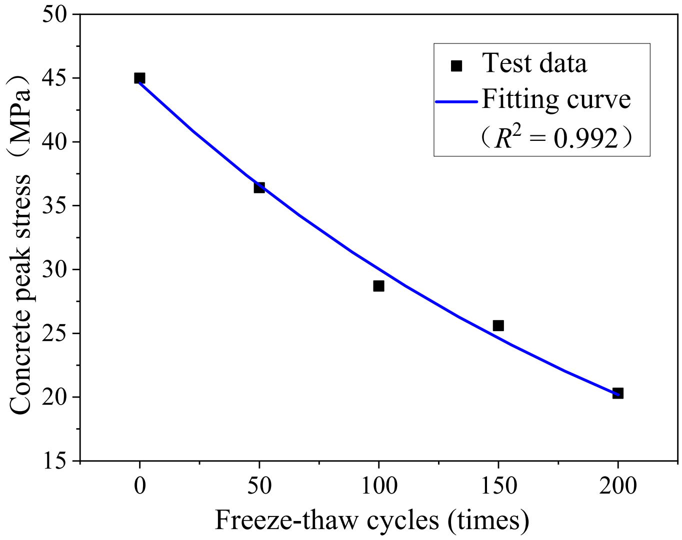

Figure 5. Fitting results for the peak stress of the concrete considering the combined action of freeze–thaw and chloride-induced corrosion.

The Mander constitutive model considers the constraint effect of the stirrups on the concrete, which can be represented by f'_l as given in Equation (22) [45]. Once the stirrups were corroded, the cross-sectional area and strength of the stirrups would be reduced, and the restraining effect of the stirrups on the concrete (i.e., the contribution of f'_l) would also be impaired. For those RC structures under the combined effects of freeze–thaw cycles and chloride-induced deterioration, the effective confining compressive stress provided by the stirrups to concrete could be expressed as

$$f'_{l,corr} = K_e \cdot \frac{2 f_y(t) \cdot A_r(t)}{d' \cdot s} \tag{26}$$

where K_e is the effective restraint factor; d' is the diameter of the stirrups; and s is the longitudinal spacing of the stirrups, respectively. By substituting Equations (25) and (26) into Equation (22), the formula of the modified peak stress of the confined concrete under the combined action of freeze–thaw cycles and chloride-induced corrosion as given in Equation (27) can be obtained.

$$f'_{cc,m} = f'_{co,m}(-1.254 + 2.254\sqrt{1 + \frac{7.49 f'_{l,corr}}{f'_{co,m}}} - 2\frac{f'_{l,corr}}{f'_{co,m}}) \tag{27}$$

(2) The modified peak strain of the confined concrete ($\varepsilon_{cc,m}$)

In the Mander constitutive model, the peak strain of the confined concrete is derived from that of the unconfined concrete. Hence, the change in the peak strain of the unconfined concrete would affect that of the confined concrete. According to the test results, the variations of the peak strain of the unconfined concrete under different freeze–thaw cycles were fitted, as shown in Figure 6.

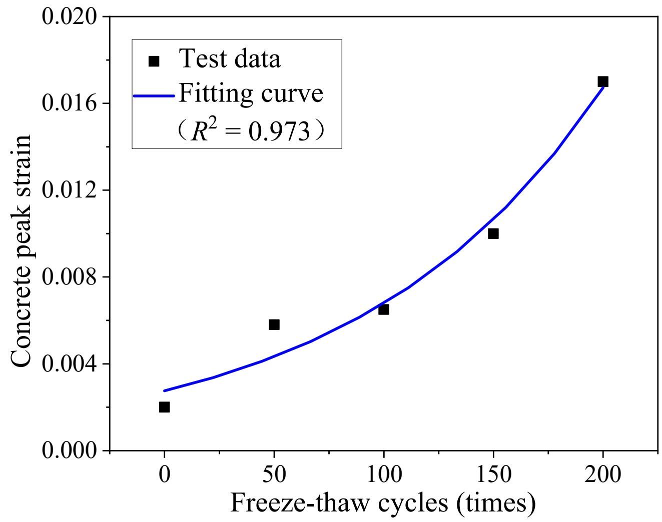

Figure 6. Fitting results for the peak strain of the concrete considering the combined action of Freeze–thaw and chloride-induced corrosion.

It can be seen from Figure 6 that the laws of the fitting results have a good match with the law of the test results of many previous studies [3,12,47]. The peak strain of the concrete increases with the increase in the number of Freeze–thaw cycles in an exponential form, which further verifies the reliability of the fitting results. Based on the fitting results in Figure 6, a function reflecting the effect of freeze–thaw cycles on the peak strain of the unconfined concrete under realistic conditions as a function of time t (years) can be expressed as

$$\varepsilon_{c,m} = 0.0002755 \cdot e^{\frac{0.009017 \cdot [N] \cdot t}{12}} \tag{28}$$

By substituting Equations (25), (27) and (28) into Equation (20), the formula of the modified peak strain of the confined concrete under the combined action of freeze–thaw cycles and chloride-induced corrosion as shown in Equation (29) can be determined.

$$\varepsilon_{cc,m} = \varepsilon_{c,m} \cdot \left[1 + 5 \cdot \left(\frac{f'_{cc,m}}{f'_{co,m}} - 1\right)\right] \tag{29}$$

(3) The modified member shape parameter (r_m)

According to the test results, the variations of the elastic modulus of the unconfined concrete under different freeze–thaw cycles were fitted, as shown in Figure 7. As seen in Figure 7, the law of the fitting results has a good matching with the law of the test results of many other scholars [46,48–50]. The elastic modulus of concrete decreases with the increase in the number of freeze–thaw cycles, and exhibits an exponential decreasing trend, which further verifies the rationality of the fitting results. Based on the fitting results in Figure 7, a function reflecting the effect of freeze–thaw cycles on the elastic modulus of the unconfined concrete under realistic conditions as a function of time t (years) is expressed as

$$E_{c,m} = 3153 \cdot e^{\frac{-0.002515 \cdot [N] \cdot t}{12}} \tag{30}$$

By substituting Equations (27), (29) and (30) into Equation (21), the formula of the modified elastic modulus of the confined concrete under the combined action of freeze–thaw cycles and chloride-induced corrosion as shown in Equation (31) can be acquired.

$$r_m = \frac{E_{c,m}}{E_{c,m} - E_{sec,m}} = \frac{E_{c,m}}{E_{c,m} - \left(\frac{f'_{cc,m}}{\varepsilon_{cc,m}}\right)} \tag{31}$$

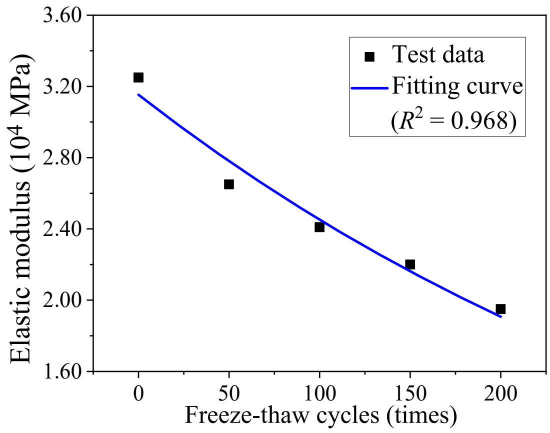

Figure 7. Fitting results for the elastic modulus of concrete considering the combined action of Freeze–thaw and chloride-induced corrosion.

3. Time-Dependent Seismic Fragility Function

Many scholars have studied the seismic fragility of RC structures [4,5,17–19,35,40,51]. Seismic fragility is usually defined as the conditional probability of the structural demand (D) exceeding the structural capacity (C) under the given ground motion intensity measure (IM), which can be expressed as

$$P[D \geq C|IM] = \Phi\left[\frac{\ln(D) - \ln(C)}{\sqrt{\beta_D^2 + \beta_C^2}}\right] \tag{32}$$

where $\Phi(\cdot)$ is the standard normal cumulative distribution function; β_D is the dispersion of the seismic demand; and β_C is the logarithmic standard deviation of the seismic capacity, respectively. It is generally known that Equation (32) represents the traditional time-invariant seismic fragility function. However, in practical engineering applications, the mechanical properties of concrete and steel rebar, and the seismic performance of RC structures may deteriorate due to the long-term freeze–thaw cycles and chloride-induced corrosion throughout their service life. As a consequence, the seismic demand and seismic capacity may vary at different service time points. Thus, the relevant time-dependent seismic fragility function can be expressed as

$$P[D(t) \geq C(t)|IM] = \Phi\left[\frac{\ln(D(t)) - \ln(C(t))}{\sqrt{\beta_{D(t)}^2 + \beta_{C(t)}^2}}\right] \tag{33}$$

This paper used the "cloud" approach to develop the probabilistic seismic demand models (PSDMs) and seismic fragility functions of RC columns. In the "cloud" approach, the seismic demand and seismic capacity are often assumed to follow the lognormal distributions [4,5,17–19,35,38,51–53]. A typical PSDM can be represented by

$$\ln(D(t)) = a(t) + b(t) \cdot \ln(IM) \tag{34}$$

where $a(t)$ and $b(t)$ are the unknown regression parameters at different time points. By substituting Equation (34) into Equation (33), the time-dependent seismic fragility function can be further expressed as

$$P[D(t) \geq C(t)|IM] = \Phi\left[\frac{a(t) + b(t) \cdot \ln(IM) - \ln C(t)}{\sqrt{\beta_{D(t)}^2 + \beta_{C(t)}^2}}\right] \tag{35}$$

Based on the above-mentioned time-dependent seismic fragility function and the proposed deterioration model of RC structures, some reasonable seismic records were selected, a full consideration of the time-dependent changes in the material properties was made, and several nonlinear time history analyses (NTHAs) were conducted. As a result, the time-dependent seismic fragility curves of RC columns under the combined action of freeze–thaw cycles and chloride-induced corrosion could be obtained accordingly, which would be discussed in detail in the following subsections.

4. Time-Dependent Seismic Fragility Analysis: Case-Study

4.1. Bridge Description and FE Modeling

To investigate the combined action of freeze–thaw cycles and chloride-induced corrosion on the time-variant mechanical properties and time-dependent seismic fragility of RC columns, a typical three-span RC continuous T-shaped girder bridge that is located in the high-latitude northern frozen coastal regions of China (i.e., Yantai city) was taken as a case study. The schematic information of the bridge is shown in Figure 8. The bridge superstructure was a 1.5 m high T-shaped girder made using C50 concrete. The substructure consisted of four double-column RC columns (made using C40 concrete) with a height of 10 m, a diameter of 1.2 m, and a steel volume ratio of approximately 7%, respectively. Both the longitudinal bars and stirrups were made from HRB335 grade steel. The bridge substructure was supported by pile foundations which were 15.6 m high. The superstructure and substructure were connected by the plate-type elastomeric bearings (PTEBs).

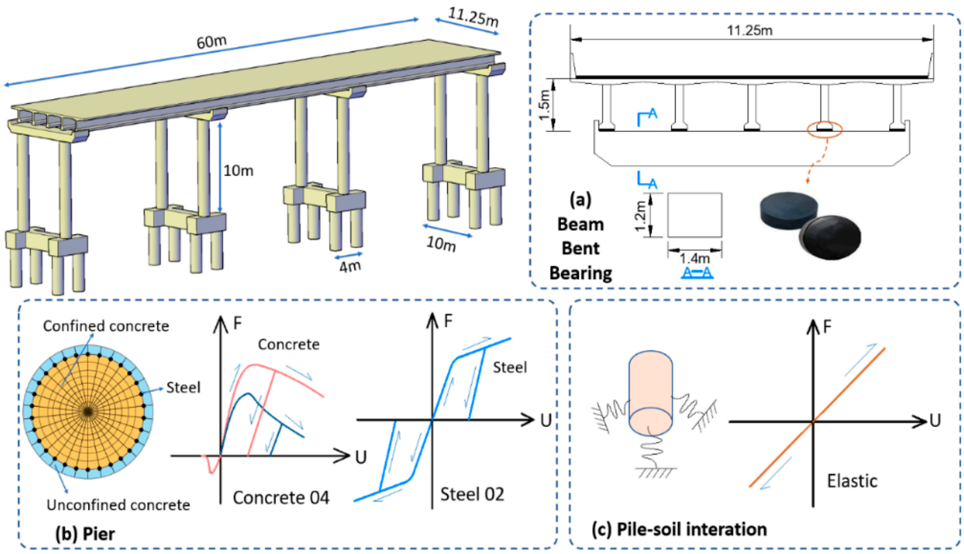

Figure 8. Schematic information of the case-study bridge. (**a**) Beam Bent Bearing; (**b**) Pier; (**c**) Pile-soil interation.

OpenSEES was used to establish the nonlinear finite element (FE) model of the case-study bridge. The bridge superstructure was simulated using the elastic beam-column element because the superstructure generally maintains elasticity during seismic events [4,5,17–19,35] according to the guidelines for the seismic design of Chinese highway bridges [54]. RC columns could be simulated using the distributed plasticity fiber element model, considering the axial force-moment interactions and nonlinear material constitutive properties (e.g., material models concrete 04 and steel 02 were used in this paper). Hence, RC columns were simulated by using the nonlinear beam-column element [4,5,17–19,35]. The fiber cross-section-based model in OpenSEES, which incorporates the nonlinear material constitutive models, was used in the plastic-hinge zones of the RC columns to simulate the plastic behaviors of RC columns under earthquake excitations [55]. In addition, the decrease in bond strength between the steel bars and concrete was not considered. The bearings (i.e., PTEBs) were simulated using the elastomeric bearing (plasticity) elements available in the OpenSEES database. In addition, to simplify the FE modeling of the bridge, the linear elastic beam-column elements were used to simulate the pile foundation, and the equivalent elastic soil springs were used to model the interaction between the soil and piles. The stiffnesses of these soil springs were determined using the "m" method according to the guidelines for the seismic design of Chinese highway bridges [54].

For those RC bridges that are located in high-latitude northern frozen coastal areas, the deterioration of RC columns caused by the combined action of freeze–thaw cycles and chloride-induced corrosion is the main factor leading to the significant reduction in their structural performance. Therefore, to simplify the analysis, this paper mainly considered the deterioration effects on the seismic performance of RC columns. Moreover, to consider the uncertainties involved in structural geometry, material performance, damping, and structural modeling, this paper considered 15 random variables to generate the seismic demand models under the combined effects of freeze–thaw cycles and chloride-induced corrosion. The statistical information of these considered random variables is summarized in Table 3.

4.2. Selection of the Ground Motions

The selection of the ground motions is integral to accurately predict the seismic response and analyzing the seismic fragility of bridge structures. According to the site conditions of the case-study bridge, this paper selected 50 natural ground motions from the PEER Ground Motion Database [56,57]. Figure 9a shows the acceleration response spectrum of the selected ground motions corresponding to a structural Rayleigh damping ratio of 5%.

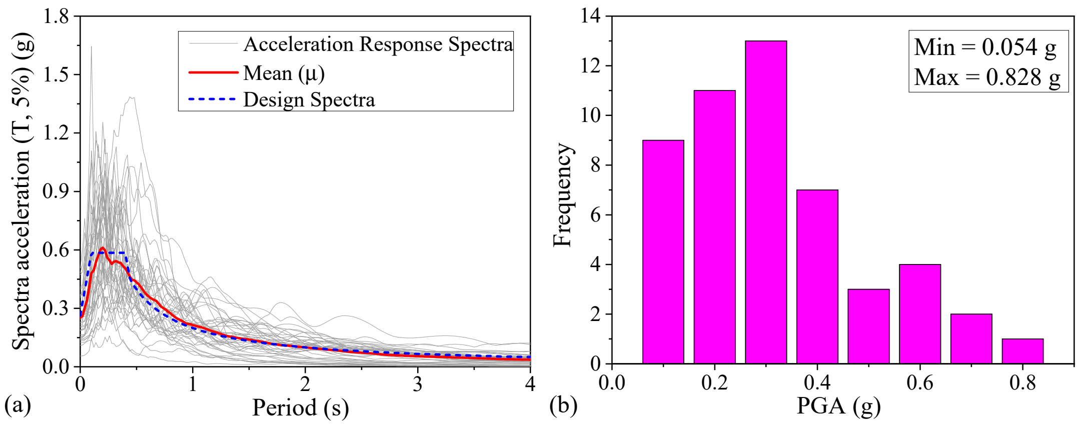

Figure 9. Acceleration spectra and PGA distribution of the selected ground motions: (**a**) acceleration spectra and (**b**) distribution of the PGA values.

As seen in Figure 9a, the mean acceleration spectrum of the selected ground motions agreed really well with the design spectrum according to the guidelines for the seismic design of Chinese highway bridges [54]. Moreover, during the seismic fragility analysis of RC structures, the selection of the appropriate intensity measure (IM) is also critical. According to [58–60], the peak ground acceleration (PGA) could effectively reflect the probabilistic seismic response of RC girder bridges. Hence, this study used PGA as the seismic IM to investigate the time-dependent seismic fragility of RC columns under the combined action of freeze–thaw cycles and chloride-induced deterioration. Figure 9b shows the frequency distribution of the PGA of the selected ground motions. As observed from Figure 9b, the selected ground motions covered a relatively broad range of PGA values. The moment magnitudes of the selected ground motions were between 5.7 and 7.2 and their source distances were between 15 and 100 km. This indicated that the selected ground motions could well represent both small and large earthquakes with different epicenter distances.

Table 3. Statistical information of the random variables considered in the FE modeling of the case-study bridge.

Parameter (Units)	Distribution	Mean	Standard Deviation	Reference
Compressive strength of the unconfined concrete (MPa)	Lognormal	30.8	6.16	[61]
Compressive strength of the confined concrete (MPa)	Lognormal	Equation (27)	0.2 mean	[62]
Peak strain of the unconfined concrete	Lognormal	0.002	0.0004	[61]
Peak strain of the confined concrete	Lognormal	Equation (29)	0.008	[62]
Ultimate compressive strain of the unconfined concrete	Lognormal	0.005	0.001	[61]
Ultimate compressive strain of the confined concrete	Lognormal	0.085	0.017	[63]
Elastic modulus of concrete (MPa)	Normal	3.24×10^4	3840	[38]
Elastic modulus of steel (MPa)	Normal	2.0×10^5	4000	[35]
Concrete cover depth (mm)	Normal	50	6	[35]
Yield strength of steel (MPa)	Lognormal	Equation (15)	0.07 mean	[61]
Bearing shear modulus (MPa)	Uniform	1.365	0.407	[40]
Rotational stiffness of the foundation (kN m/rad)	Uniform	1.8×10^7	5.2×10^6	[63]
Translation stiffness of foundation (kN/m)	Uniform	6.2×10^5	1.5×10^5	[63]
Deck mass ratios	Uniform	1.0	0.058	[40]
Damping ratio	Normal	0.045	0.0125	[40]

4.3. Time-Dependent Seismic Fragility Analysis of the Aging RC Columns

4.3.1. Corrosion Initiation Time of Steel Rebar (t_{corr})

In this section, the proposed deterioration model of RC structures and time-dependent seismic fragility function were used to study the timed-dependent seismic fragility of the aging RC columns exposed to the combined action of freeze–thaw cycles and chloride-induced corrosion. Firstly, the corrosion initiation time of the steel reinforcements can be determined by using Equation (9) in Section 2.3. For the RC columns of the case-study bridge, the concrete protective layer thickness was 50 mm; the measured number of freeze–thaw cycles in the marine splash zone was 2.9 per year; the measured concentration of chloride ion on the concrete surface (C_s) was 0.548%; the measured concrete chloride ion diffusion coefficient (D_{ref}) at the default 28 days was 2.69 × 10–12 m^2/s; the critical chloride concentration (C_{cr}) was 0.05%; and the decaying parameter (m) was 0.2, respectively. By substituting these parameters into Equation (9), the following equation (Equation (36)) could be obtained. Solving this equation through the numerical iterations, the corrosion initiation time of steel rebar (t_{corr}) was approximately 11.02 years of their service period under the combined action of freeze–thaw cycles and chloride-induced deterioration.

$$0.05\% = 0.548\% \times \left(1 - erf\frac{0.05}{2\sqrt{0.51 \times 10^{-4} \cdot t_{corr}{}^{0.8} \cdot e^{0.02117 \cdot t_{corr}}}}\right) \tag{36}$$

4.3.2. Time-Dependent Mechanical Properties of the Steel Rebar

Based on the proposed deterioration model of RC structures under the combined action of freeze–thaw cycles and chloride-induced corrosion, the time-variant mechanical properties of steel rebar could be obtained. Since the effective confining stress of the confined concrete is mainly contributed by the stirrups, the time-dependent cross-sectional area and yield strength of the stirrups are shown in Figure 10.

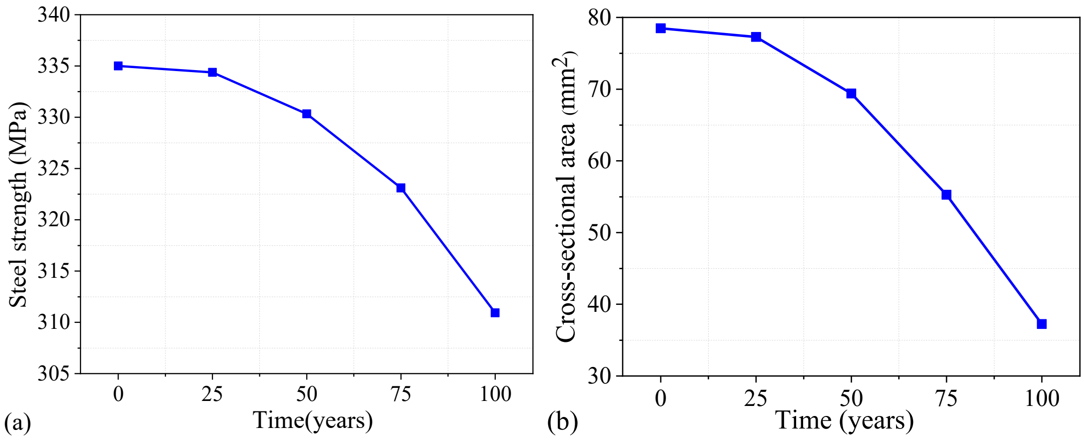

Figure 10. Time-dependent material properties of the stirrups: (**a**) yield strength and (**b**) cross-sectional area.

As seen in Figure 10, both the cross-sectional area and yield strength of the stirrups were gradually reduced over time under the combined action of freeze–thaw cycles and chloride-induced deterioration, and the reduction ratio of yield strength was relatively lesser than that of the cross-sectional area. For example, compared to that of the pristine RC columns, the cross-sectional area of the stirrups in the 50-year-corroded RC columns degraded by 11.6%, whereas that in the 100-year-corroded RC columns decreased by 52.5%. In addition, compared with the as-built RC columns, the yield stress of the stirrups in the 100-year-corroded columns only decreased by 7.2%. These observations suggested that the combined action of freeze–thaw cycles and chloride-induced corrosion seriously deteriorated the mechanical properties of the stirrups.

4.3.3. Time-Dependent Mechanical Properties of the Concrete

Similarly, based on the proposed deterioration model of RC structures as introduced in Section 2, the time-variant mechanical properties of concrete could also be acquired in this part. Figure 11 shows the time-variant peak strains and peak stresses of both the confined and unconfined concrete, respectively. As seen in Figure 11a, compared to the pristine RC columns, the peak stresses of the confined and unconfined concrete decreased by 42.9% and 44%, respectively, after 50 years of service, indicating that the combined action of freeze–thaw cycles and chloride-induced corrosion had a relatively more significant effect on the peak stress of the unconfined concrete as expected. This could be attributed to the lateral confining stress contributed by the transverse stirrups to the confined concrete being larger than that of the unconfined concrete. On the contrary, as seen in Figure 11b, compared to the as-built RC columns, the peak strains of the confined and unconfined concrete increased by 5.5 times and 5.1 times, respectively, after 50 years of service. This indicated that the peak strain of the RC columns would increase with the increase in service time, then the deformation capacity of the column would deteriorate due to the combined action of freeze–thaw cycles and chloride-induced corrosion.

According to the aforementioned discussions, the combined action of freeze–thaw cycles and chloride-induced corrosion had negative effects on the deformation capability and ultimate load-carrying ability of RC columns. Meanwhile, the deterioration effect on the deformation capability tended to be more significant than that on the ultimate load-carrying ability of RC columns. However, RC girder bridges mainly dissipate the energy produced by earthquakes through the plastic deformation of RC columns. Therefore, it is necessary to carefully consider the deterioration effects on the mechanical properties and seismic performance of the aging RC columns caused by the combined action of freeze–thaw cycles and chloride-induced corrosion, particularly for those RC bridges that are located in the northern frozen coastal regions.

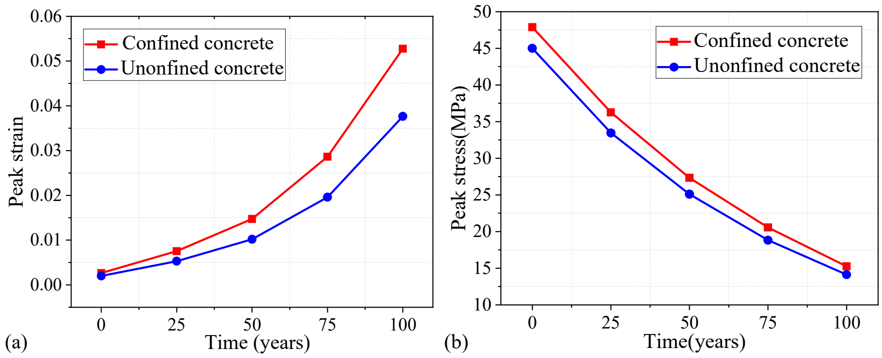

Figure 11. Time-dependent material properties of the confined and unconfined concrete: (**a**) the peak strain and (**b**) the peak stress.

4.3.4. Time-Dependent Seismic Fragility Curves of RC Columns

Considering the derived uncertainties of the considered random parameters listed in Table 3, 50 FE models of the case-study bridge were generated using the uniform design method [4,5,17–19,35,40]. The considered RC columns had a relatively large slenderness ratio, which satisfies the requirements of the ductile seismic design, and therefore avoids possible shear failure during the seismic events. Therefore, bending failure was the main failure mode of the considered RC columns in this paper. This study only studied the longitudinal seismic response of the curvature demand (φ) of the RC columns, which is one of the most common damage measurements in the seismic vulnerability analyses of RC bridges [35,40]. Regression analyses were performed using Equation (34) to obtain the PSDMs of RC columns under different service periods (i.e., 0, 25, 50, 75, and 100 years, respectively). The results are shown in Table 4.

Table 4. PSDMs of the aging RC columns.

Time (Years)	PSDM	R^2	$\beta_{D\mid PGA}(t)$
0	$\ln(\varphi) = -4.014 + 1.038 \cdot \ln(PGA)$	0.761	0.386
25	$\ln(\varphi) = -3.965 + 1.087 \cdot \ln(PGA)$	0.752	0.392
50	$\ln(\varphi) = -3.753 + 1.056 \cdot \ln(PGA)$	0.764	0.435
75	$\ln(\varphi) = -3.502 + 1.059 \cdot \ln(PGA)$	0.735	0.457
100	$\ln(\varphi) = -3.267 + 1.096 \cdot \ln(PGA)$	0.719	0.483

Moreover, during the seismic fragility estimates of a typical RC column, four different damage states are generally defined according to the possible ductility levels of RC columns [4,5,17–19,35,40], including (i) slight damage state; (ii) moderate damage state; (iii) extensive damage state; and (iv) complete damage state. Finally, Figure 12 shows the time-dependent seismic fragility curves of the aging RC columns subjected to the combined action of freeze–thaw cycles and chloride-induced corrosion under different damage states, respectively.

As seen in Figure 12, the failure probabilities of RC columns under different damage states (i.e., slight, moderate, extensive, and complete damage states) exhibited an increasing trend with the increase in their service period. This suggested that the combined action of freeze–thaw cycles and chloride-induced corrosion would lead to the deterioration of the seismic performance and seismic fragilities of RC columns, and then further impair the durability and service ability of the bridge structures. In addition, as observed from Figure 12, the time-dependent seismic fragility of the aging RC columns exhibited a nonlinear increasing trend with the increase in the intensity levels of the defined damage states. For example, compared to that of the pristine columns, under a PGA of 0.15 g, the failure probabilities of the 100-year-corroded columns increased by 80.7% and 185% under the slight and moderate damage states, respectively. However, compared to the as-built RC columns, under a PGA of 0.85 g, the seismic fragilities of the 100-year-corroded columns increased by 99.8% and 751% under the extensive and complete damage states, respectively. Moreover, a nonlinear increase in the time-dependent seismic fragility of RC columns with the increase in service life could be also observed under different damage states. In other words, in the initial 25 years of service, the failure probability of RC columns under different damage states did not increase significantly due to the relatively slow and slight deterioration of the mechanical properties of the materials. However, in the latter service ranges of RC columns, once the concrete was cracked and the steel reinforcements began to being corroded, the seismic fragility of RC columns under different damage states increased rapidly owing to the combined action freeze–thaw cycles and chloride-induced corrosion.

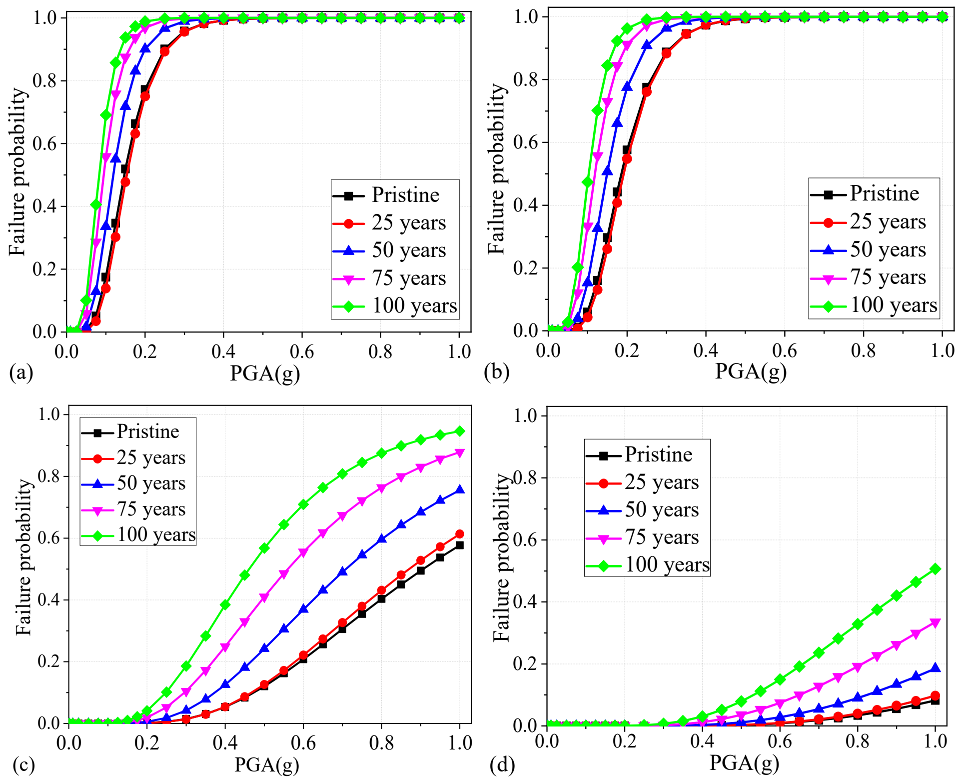

Figure 12. Time-dependent seismic fragility curves of RC columns at different damage states: (**a**) slight; (**b**) moderate; (**c**) extensive; and (**d**) complete damage states.

5. Conclusions

To investigate the combined effects of freeze–thaw cycles and chloride-induced corrosion on the time-dependent mechanical properties, seismic performance, and seismic fragilities of the aging RC columns, this paper conducted a series of concrete deterioration tests under the combined action of freeze–thaw cycles and chloride-induced deterioration. The variation law of the chloride ion diffusion coefficient with the number of freeze–thaw cycles was also studied through the chloride ion permeability tests in a laboratory. By considering the difference between the laboratory conditions and the conditions of the areas in which the RC columns were located, a conversion relationship between the number of freeze–thaw cycles in the laboratory conditions and the average annual freeze–thaw cycles of the practical regions was considered. According to the experimental results, a time-variant deterioration model of RC structures under the combined action of freeze–thaw cycles and chloride-induced corrosion was developed.

In addition, based on the established deterioration model of RC structures, this paper proposed a time-dependent seismic fragility assessment framework considering the uncertainties involved in the structural geometrics and mechanical properties of the materials, and ground motions. By taking a representative three-span RC continuous T-shaped girder bridge that is located in the northern frozen coastal areas of China as a case study, the time-dependent seismic fragility estimates of RC columns under the combined action of freeze–thaw cycles and chloride-induced deterioration were carried out. The results indicated that the combined action of freeze–thaw cycles and chloride-induced corrosion could seriously deteriorate both the mechanical properties and seismic performance of the aging RC columns. Moreover, the time-dependent seismic fragility of the deteriorating RC columns exhibited a nonlinear increase with the increase in their service years and the intensity levels of the defined limit states.

Moreover, this study comprehensively investigated the deterioration effects on the time-variant mechanical properties, seismic performance, and seismic vulnerabilities of the aging RC columns caused by the combined action of freeze–thaw damage and chloride-induced corrosion for the first time. Therefore, this paper could provide some possible references for decision makers and engineers for the maintenance and rehabilitation of the deteriorating RC columns of highway bridges that are located in the high-latitude northern frozen coastal regions. Furthermore, in this paper, during the time-dependent seismic fragility analysis of the aging RC columns, the influence of the combined action of freeze–thaw cycles and chloride-induced corrosion on the mechanical properties of the concrete and steel reinforcements was mainly considered, whereas the influence of the decrease in bond strength between the reinforcements and concrete was not analyzed. In future work, relevant freeze–thaw damage tests would be further carried out to study the variation laws of the bond strength between the steel reinforcements and concrete. Additionally, the refined simulation of the plastic hinge of RC structures will also be a key element in future research. Meanwhile, further tests on the combined action of freeze–thaw cycles and chloride-induced corrosion should be carried out with more test samples to establish a more reasonable probabilistic deterioration model for the design office to use.

Author Contributions: Conceptualization, F.C. and H.L.; methodology, F.C. and H.L.; software, L.S.; validation, F.C., L.S., X.W. and M.L.; formal analysis, L.S., X.W., M.L. and P.H.; investigation, L.S., X.W., M.L. and P.H.; resources, F.C. and S.D.; data curation, M.L. and X.Z.; writing—original draft preparation, F.C., L.S., X.W., M.L. and P.H.; writing—review and editing, H.L.; visualization, M.L., S.D. and X.Z.; supervision, F.C. and H.L.; project administration, F.C. and S.D.; funding acquisition, F.C. and S.D. All authors have read and agreed to the published version of the manuscript.

Funding: The research described in this paper was supported by the "Shandong Natural Science Foundation Project" (Project No. 60000101032); the National Natural Science Foundation of China (Grant No. 52108211); Hunan Provincial Department of Education (No. 21B0188); and the Natural Science Foundation of Hunan Province (No. 2022JJ40186). The authors greatly acknowledge their financial supports.

Data Availability Statement: All data is included in the paper, so this can be exclude.

Acknowledgments: The research described in this paper was supported by the "Shandong Natural Science Foundation Project" (Project No. 60000101032); the National Natural Science Foundation of China (Grant No. 52108211); Hunan Provincial Department of Education (No. 21B0188); and the Natural Science Foundation of Hunan Province (No. 2022JJ40186). The authors greatly acknowledge their financial supports.

Conflicts of Interest: The authors declare that they have no known competing financial interest or personal relationship that could have appeared to influence the work reported in this paper.

References

1. Duan, A.; Tian, Y.; Dai, J.; Jin, W. A stochastic damage model for evaluating the internal deterioration of concrete due to freeze–thaw action. *Mater. Struct.* **2014**, *47*, 1025–1039. [CrossRef]
2. Si, Z.; Du, X.; Huang, L.; Li, Y. Meso-scale failure of freezing–thawing damage of concrete under uniaxial compression. *Appl. Sci.* **2020**, *10*, 1252. [CrossRef]
3. Qiu, J.; Zhou, Y.; Vatin, N.; Guan, X.; Sultanov, S.; Khemarak, K. Damage constitutive model of coal gangue concrete under freeze-thaw cycles. *Constr. Build. Mater.* **2020**, *264*, 120720. [CrossRef]
4. Li, H.; Li, L.; Li, W.; Xu, L. Seismic fragility assessment framework for highway bridges based on an improved uniform design-response surface model methodology. *Bull. Earthq. Eng.* **2020**, *18*, 2329–2353. [CrossRef]

5. Li, H.; Li, L.; Zhou, G.; Xu, L. Effects of various modeling uncertainty parameters on the seismic response and seismic fragility estimates of the aging highway bridges. *Bull. Earthq. Eng.* **2020**, *18*, 6337–6373. [CrossRef]
6. Cao, D.; Zhao, M.; Ge, W.; Wang, B. Experimental study on the eccentric compressive behaviors of RC columns after freeze-thaw cycles. *Recent Adv. Mater. Anal. Monit. Eval. Found. Bridge Eng.* **2014**, 38–45.
7. Liu, K.; Yan, J.; Zou, C. A pilot experimental study on seismic behavior of recycled aggregate concrete columns after freeze-thaw cycles. *Constr. Build. Mater.* **2018**, *164*, 497–507. [CrossRef]
8. Xu, S.; Li, A.; Ji, Z.; Wang, Y. Seismic performance of reinforced concrete columns after freeze-thaw cycles. *Constr. Build. Mater.* **2016**, *102*, 861–871. [CrossRef]
9. Hanjari, K. Structural Behaviour of Deteriorated Concrete Structures. Ph.D. Thesis, Chalmers University of Technology-Department of Civil and Environmental Engineering-Division of Structural Engineering, Gothenburg, Sweden, 2010.
10. Zheng, S.; Zhang, Y.; Pei, P. Experimental study on the seismic performance of reinforced concrete columns under freeze-thaw cycles. *J. Build. Struct.* **2020**, *41*, 84–91.
11. Hasan, M.; Okuyama, H.; Sato, Y.; Ueda, T. Stress-strain model of concrete damaged by freezing and thawing cycles. *J. Adv. Concr. Technol.* **2004**, *2*, 89–99. [CrossRef]
12. Berto, L.; Saetta, A.; Talledo, D. Constitutive model of concrete damaged by freeze–thaw action for evaluation of structural performance of RC elements. *Constr. Build. Mater.* **2015**, *98*, 559–569. [CrossRef]
13. Shen, X.; Jiang, W.; Hou, D.; Hou, D.; Hu, Z.; Yang, J.; Liu, Q. Numerical study of carbonation and its effect on chloride binding in concrete. *Cem. Concr. Compos.* **2019**, *104*, 1031–1045. [CrossRef]
14. Guo, A.; Li, H.; Ba, X.; Guan, X.; Li, H. Experimental investigation on the cyclic performance of reinforced concrete piers with chloride-induced corrosion in marine environment. *Eng. Struct.* **2015**, *105*, 1–11. [CrossRef]
15. Ou, Y.; Fan, H.; Nguyen, N. Long-term seismic performance of reinforced concrete bridges under steel reinforcement corrosion due to chloride attack. *Earthq. Eng. Struct. Dyn.* **2013**, *42*, 2113–2127. [CrossRef]
16. Akiyama, M.; Frangopol, D.; Matsuzaki, H. Life-cycle reliability of RC bridge piers under seismic and airborne chloride hazards. *Earthq. Eng. Struct. Dyn.* **2011**, *40*, 1671–1687. [CrossRef]
17. Li, H.; Li, L.; Zhou, G.; Xu, L. Time-dependent seismic fragility assessment for aging highway bridges subject to non-uniform chloride-induced corrosion. *J. Earthq. Eng.* **2022**, *26*, 3523–3553. [CrossRef]
18. Li, H.; Li, L.; Xu, L. Seismic Response and Fragility Estimates of Highway Bridges Considering Various Modeling Uncertainty Parameters. In *Advancements in Geotechnical Engineering*; Springer: Cham, Switzerland, 2021; pp. 31–53.
19. Li, H.; Li, L. Bridge fragility analysis based on an improved uniform design-response surface methodology. *J. Vib. Shock.* **2018**, *37*, 245–254.
20. Wang, B.; Huang, W.; Zheng, S. Study on restoring force performance of corrosion damage steel frame beams under acid atmosphere. *Appl. Sci.* **2018**, *9*, 103. [CrossRef]
21. Val, D.; Stewart, M.; Melchers, R. Effect of reinforcement corrosion on reliability of highway bridges. *Eng. Struct.* **1998**, *20*, 1010–1019. [CrossRef]
22. GB/T 50082-2009. Long-term Performance and Durability of Ordinary Concrete. Ministry of Housing and Urban-Rural Development of China: Beijing, China, 2009.
23. Chatterji, S. On the applicability of Fick's second law to chloride ion migration through Portland cement concrete. *Cem. Concr. Res.* **1995**, *25*, 299–303. [CrossRef]
24. Zhang, J.; Wang, J.; Kong, D. Chloride diffusivity analysis of existing concrete based on Fick's second law. *J. Wuhan Univ. Technol.-Mater. Sci. Ed.* **2010**, *25*, 142–146. [CrossRef]
25. Liu, J.; Jia, Y.; Wang, J. Calculation of chloride ion diffusion in glass and polypropylene fiber-reinforced concrete. *J. Constr. Build. Mater.* **2019**, *215*, 875–885. [CrossRef]
26. Wang, Y.; An, M.; Yu, Z.; Han, B.; Ji, W. Experimental and cellular-automata-based analysis of chloride ion diffusion in reactive powder concrete subjected to freeze–thaw cycling. *Constr. Build. Mater.* **2018**, *172*, 760–769. [CrossRef]
27. Zhang, Y.; Zhang, J.; Luo, W.; Wang, J.; Shi, J.; Zhuang, H.; Wang, Y. Effect of compressive strength and chloride diffusion on life cycle CO_2 assessment of concrete containing supplementary cementitious materials. *J. Clean. Prod.* **2019**, *218*, 450–458. [CrossRef]
28. Ma, J.; Lin, P. Simulation approach for random diffusion of chloride in concrete under sustained load with cellular automata. *Materials* **2022**, *15*, 4384. [CrossRef]
29. Wang, Y.; Kun, F. Comparisons of instantaneous chloride diffusion coefficients determined by RCM method and chloride natural diffusion test. *Constr. Build. Mater.* **2019**, *223*, 595–604. [CrossRef]
30. Violetta, B. Life-365 service life prediction model. *Concr. Int.* **2002**, *24*, 53–57.
31. Ge, Y.; Yuan, J.; Yang, W. Influence of freeze-thaw action on bond strength, carbonation and chloride diffusion coefficient of air-entraining concrete. *J. Highw. Transp. Res. Dev.* **2010**, *27* (Suppl. S1), 103–105.
32. Wang, Y.; Liu, Z.; Fu, K.; Li, Q.; Wang, Y. Experimental studies on the chloride ion permeability of concrete considering the effect of freeze–thaw damage. *Constr. Build. Mater.* **2020**, *236*, 117556. [CrossRef]
33. Wang, D.; Zhou, X.; Fu, B.; Zhang, L. Chloride ion penetration resistance of concrete containing fly ash and silica fume against combined freezing-thawing and chloride attack. *Constr. Build. Mater.* **2018**, *169*, 740–747. [CrossRef]
34. Li, J.; Wang, Z. Quantitative design of concrete frost resistance. *Concrete* **2000**, *9*, 61–64.
35. Cui, F.; Zhang, H.; Ghosn, M.; Xu, Y. Seismic fragility analysis of deteriorating RC bridge substructures subject to marine chloride-induced corrosion. *Eng. Struct.* **2018**, *155*, 61–72. [CrossRef]

36. Liu, T.; Weyers, R. Modeling the dynamic corrosion process in chloride contaminated concrete structures. *Cem. Concr. Res.* **1998**, *28*, 365–379. [CrossRef]
37. Guo, Y.; Trejo, D.; Yim, S. New model for estimating the time-variant seismic performance of corroding RC bridge columns. *J. Struct. Eng.* **2015**, *141*, 1–12. [CrossRef]
38. Vu, K.; Stewart, M. Structural reliability of concrete bridges including improved chloride-induced corrosion models. *Struct. Saf.* **2000**, *22*, 313–333. [CrossRef]
39. Du, Y.; Clark, L.; Chan, A. Residual capacity of corroded reinforcing bars. *Mag. Concr. Res.* **2005**, *57*, 135–147. [CrossRef]
40. Cui, F.; Li, H.; Dong, X.; Wang, B.; Li, J.; Xue, H.; Qi, M. Improved time-dependent seismic fragility estimates for deteriorating RC bridge substructures exposed to chloride attack. *Adv. Struct. Eng.* **2021**, *24*, 437–452. [CrossRef]
41. Shopov, A.; Bonev, B. Ascertainment of the change of the ductility in corroded steel specimens by experiment. *Int. J. Civ. Eng. Technol.* **2019**, *10*, 1551–1560.
42. Mander, J.; Priestley, M.; Park, R. Theoretical stress-strain model for confined concrete. *J. Struct. Eng.* **1988**, *114*, 1804–1826. [CrossRef]
43. Orakcal, K.; Massone, L.; Ulugtekin, D. A hysteretic constitutive model for reinforced concrete panel elements. *Int. J. Concr. Struct. Mater.* **2019**, *13*, 51. [CrossRef]
44. Sun, L.; Jiang, K.; Zhu, X.; Xu, L. An alternating experimental study on the combined effect of freeze-thaw and chloride penetration in concrete. *Constr. Build. Mater.* **2020**, *252*, 119025. [CrossRef]
45. Yang, D.; Yan, C.; Liu, S.; Ju, Z.; Hu, Z. Stress-strain constitutive model of concrete corroded by saline soil under uniaxial compression. *Constr. Build. Mater.* **2019**, *213*, 665–674. [CrossRef]
46. Qiu, W.; Teng, F.; Pan, S. Damage constitutive model of concrete under repeated load after seawater freeze-thaw cycles. *Constr. Build. Mater.* **2020**, *236*, 1154–1171. [CrossRef]
47. Zhang, D.; Mao, M.; Zhang, S.; Yang, Q. Influence of stress damage and high temperature on the freeze–thaw resistance of concrete with fly ash as fine aggregate. *Constr. Build. Mater.* **2019**, *229*, 1168–1179. [CrossRef]
48. Li, B.; Mao, J.; Nawa, T.; Han, T. Mesoscopic damage model of concrete subjected to freeze-thaw cycles using mercury intrusion porosimetry and differential scanning calorimetry (MIP-DSC). *Constr. Build. Mater.* **2017**, *147*, 79–90. [CrossRef]
49. Sun, M.; Xin, D.; Zou, C. Damage evolution and plasticity development of concrete materials subjected to freeze-thaw during the load process. *Mech. Mater.* **2019**, *139*, 576–594. [CrossRef]
50. Gong, X.; Yu, H.; Wu, C. Research on the constitutive relationship of concrete under uniaxial compression in freeze–thaw environment. *Constr. Build. Mater.* **2022**, *336*, 127543. [CrossRef]
51. Tavares, D.; Padgett, J.; Paultre, P. Fragility curves of typical as-built highway bridges in eastern Canada. *Eng. Struct.* **2012**, *40*, 107–118. [CrossRef]
52. Cornell, C.; Jalayer, F.; Hamburger, R.; Foutch, D. Probabilistic basis for 2000 SAC federal emergency management agency steel moment frame guidelines. *J. Struct. Eng.* **2002**, *128*, 526–533. [CrossRef]
53. Choi, E.; DesRoches, R.; Nielson, B. Seismic fragility of typical bridges in moderate seismic zones. *Eng. Struct.* **2004**, *26*, 187–199. [CrossRef]
54. JTG/T B02-01. Seismic Design Rules for Highway Bridges in China. Ministry of Transport of the People's Republic of China: Beijing, China, 2008.
55. Li, L.; Luo, G.; Wang, Z.; Zhang, Y.; Yan, Z. Prediction of residual behaviors for post-earthquake damaged reinforced concrete column based on damage distribution model. *Eng. Struct.* **2021**, *234*, 111927. [CrossRef]
56. Stewart, J.; Douglas, J.; Javanbarg, M.; Bozorgnia, Y.; Abrahamson, N.A.; Boore, D.M.; Campbelle, K.W.; Delavaud, E.; Erdik, M.; Stafford, P.J. Selection of ground motion prediction equations for the global earthquake model. *Earthq. Spectra* **2015**, *31*, 19–45. [CrossRef]
57. Li, H.; Zhou, G.; Wang, J. Selection of Ground Motion Intensity Measures and Evaluation of the Ground Motion-Related Uncertainties in the Probabilistic Seismic Demand Analysis of Highway Bridges. *Buildings* **2022**, *12*, 56–75. [CrossRef]
58. JTG/T 2231-01. Code for Seismic Design of Highway Bridges. Ministry of Transport of the People's Republic of China: Beijing, China, 2020.
59. Nielson, B.; DesRoches, R. Seismic fragility methodology for highway bridges using a component level approach. *Earthq. Eng. Struct. Dyn.* **2007**, *36*, 823–839. [CrossRef]
60. Li, Q.; Huang, L.; Ye, H.; Fu, C.; Jin, X. Mechanical degradation of reinforced concrete columns corroded under sustained loads. *Int. J. Civ. Eng.* **2020**, *18*, 883–901. [CrossRef]
61. Pan, Y.; Agrawal, A.; Ghosn, M. Seismic fragility of continuous steel highway bridges in New York State. *J. Bridge Eng.* **2007**, *12*, 689–699. [CrossRef]
62. Thanapol, Y.; Akiyama, M.; Frangopol, D. Updating the seismic reliability of existing RC structures in a marine environment by incorporating the spatial steel corrosion distribution: Application to bridge piers. *J. Bridge Eng.* **2016**, *21*, 1–17. [CrossRef]
63. Barbato, M.; Gu, Q.; Conte, J. Probabilistic push-over analysis of structural and soil-structure systems. *J. Struct. Eng.* **2010**, *136*, 1330–1341. [CrossRef]